Tetrahedron 69 (2013) 7290–7299

Contents lists available at SciVerse ScienceDirect

Tetrahedron

journal homepage: www.elsevier.com/locate/tet

Functionalized oligothiophene-based heterocyclic aromatic fluorescent compounds with various donor–acceptor spacers and adjustable electronic properties: a theoretical and experimental perspective

Tao Tao [a], Hui-Fen Qian [a,b], Kun Zhang [a], Jiao Geng [a], Wei Huang [a,*]

[a] State Key Laboratory of Coordination Chemistry, Nanjing National Laboratory of Microstructures, School of Chemistry and Chemical Engineering, Nanjing University, Nanjing, Jiangsu Province, 210093, PR China
[b] College of Sciences, Nanjing University of Technology, Nanjing, Jiangsu Province, 210009, PR China

ARTICLE INFO

Article history:
Received 24 April 2013
Received in revised form 4 June 2013
Accepted 21 June 2013
Available online 29 June 2013

Keywords:
Oligothiophenes
Syntheses
Photophysics
Electrochemistry
DFT study

ABSTRACT

Syntheses, characterizations, optical, electrochemical, and thermal properties of a family of linear oligothiophene-based heterocyclic aromatic fluorescent compounds are described herein. They all have effective π-conjugated systems with D–π–D or A–π–A structures as well as different bromo, thiocyano, formyl, and triphenylamino tails. X-ray single-crystal structure of **2TPA2T** methanol semisolvate reveals a trans configuration with different dihedral angles between adjacent aromatic heterocycles. Theoretical and experimental studies have been made to reveal the differences from related compounds with adjustable electronic properties. The influences of introducing different D/A functionalized tails on the band-gap convergence have also been discussed, where the convergence behavior corrected via the thienyl ring coefficient (n_{corr}) shows better correlation of linear fitting based on the extrapolation of HOMO–LUMO gaps at the B3LYP/6-31G* level.

1. Introduction

Research on the π-functional materials,[1] such as thiophene-based and fluorene-based molecules and polymers, has been attracting considerable interests in view of their wide applications on organic semiconducting materials and electronic devices, such as dye-sensitized solar cells (DSSCs),[2] organic solar cells (OSCs),[3] organic light-emitting diodes (OLEDs),[4] organic field-effect transistors (OFETs),[5] chemosensors,[6] biosensors,[7] and electrochromic devices.[8] In particular, linear conjugated oligomers[9] share many of the properties of conjugated polymers with certain advantages including their well-defined chemical structures, monodispersity, better solubility, easier purification, fewer defects, and the possibility to introduce versatile functionalities. However, rational design and synthesis of extended heterocyclic aromatic systems for constructing high-performance electronic materials are still very important and challenging issues.

Limited by the tremendous gap that still exists between the structures and the properties, these problems have not been completely solved. Up till now, many theoretical and experimental efforts[1,9] have been made on the studies of a variety of linear conjugated oligomers. From the basic research perspective, exploration of the convergence behavior[9,10] is helpful for understanding the differences from short conjugated oligomers to polymers whose properties are calculated by the extrapolation of oligomeric properties to infinite chain lengths in theory. Meanwhile, an effective strategy for designing experimentally low band-gap oligomers is to use the miscellaneous conjugated donor–acceptor (D–A) concept because different D–A units in the linear aromatic heterocyclic semiconducting compounds show different band gaps.[11] On the one hand, the so-called core-embedded method[12] can be finely tuned from the structure to the property, such as size, symmetry, conformation, coordination site, dihedral angle between adjacent aromatic heterocycles, the HOMO–LUMO gap, linear absorbance, fluorescence and electrochemical properties, solubility and reaction activity by introducing different alkyl substituted groups. For instance, core-substituted naphthalene diimides with tunable emission wavelengths are reported for fluorescence resonance energy transfer studies by Würthner et al.[13] Namely, the alkoxy-substituted derivatives are yellow dyes with green emission and low photoluminescence quantum yields, whereas the amine-substituted derivatives exhibit a color range from red to blue with strong photoluminescence quantum yields up to 76%. On the

* Corresponding author. E-mail address: whuang@nju.edu.cn (W. Huang).

0040-4020/$ – see front matter © 2013 Elsevier Ltd. All rights reserved.
http://dx.doi.org/10.1016/j.tet.2013.06.087

other hand, the introduction of a functional terminal group[14] into oligothiophenes provides an opportunity for incorporating the π-conjugated system covalently into a more complex system. For example, π-conjugated oligomers, based on benzothiadiazole and thiophene, increasing and decreasing the donor and acceptor strengths, are reported for nonlinear optics and near-IR emission by the Reynolds' group.[15] For many applications, such as OLEDs and photovoltaics, the HOMO–LUMO gap is critical to an optimized device because it determines the color of the light emitted for an OLED or the monochromatic incident photon-to-electron conversion efficiency for a photovoltaic device.

Taking all the above-mentioned factors into consideration, it is believed that the linear oligothiophene-based heterocyclic aromatic fluorescent compounds, bearing delocalized π-systems, versatile D–A hybrids, and functionalized terminal groups, are good candidates for the investigations on the design and synthesis of π-conjugated oligomers from a theoretical and experimental perspective. In our previous work, a family of 1,10-phenanthroline- and bithiazole-based heterocyclic aromatic compounds with terminal thienyl, imidazolyl, pyridyl groups has been described.[16] Furthermore, temperature-dependent semiconducting and photoresponsive properties of self-assembled nanocomposite films and nanodevices fabricated from these compounds and their metal complexes have been explored.[17] Herein we have extended our work on the oligothiophene-centered semiconducting and fluorescent compounds where terminal bromo, thiocyano, formyl, and triphenylamino groups are successfully introduced (Scheme 1). The syntheses and full characterizations of this family of linear heterocyclic aromatic compounds with various electron-donating and electron-withdrawing tails have been described, and the aim of combining various donor and acceptor substituents into molecules is to finely tune their electronic structures and compare their spectroscopic, electrochemical, and thermal properties.

number of aromatic heterocycles and the electronic and fluorescent spectra, band-gap alterations, the limitation of solubility of compounds, which is also influenced by the substituent effects. So theoretical and experimental studies have been made to reveal the differences from 42 related compounds (Scheme 2) with adjustable electronic properties, where the influences of introducing seven types of functionalized terminals (i.e., proton, bromo, imidazolyl, pyridyl, thiocyano, formyl, and triphenylamino groups) and the number of aromatic heterocycles (n=1–6) on the convergence behavior of HOMO–LUMO gaps have been included. It is found that convergence behavior corrected via the thienyl ring coefficient (n_{corr}) shows better correlation of linear fitting, which is based on the extrapolation of HOMO–LUMO gaps at the B3LYP/6-31G* level.

2. Results and discussion

2.1. Syntheses and spectral characterizations

As shown in Scheme 2, 42 model compounds were involved in the systematic comparisons for a theoretical and experimental perspective in terms of band-gap engineering. Among them, 31 of them are known compounds including 7 new compounds in this work and the other 11 compounds are unreported. Our synthetic strategy was based on the routes shown in Scheme 1, in which the starting materials 3,3″-dimethyl-2,2′:5′,2″-terthiophene (**3T-Me**) and 3,3‴-dimethyl-2,2′:5′,2″:5″,2‴-quaterthiophene (**4T-Me**) were prepared according to our previously reported approaches.[16c] All the target compounds were prepared by carbon–carbon (C–C) bond and/or carbon–nitrogen (C–N) bond cross-coupling reactions. The combination of different cross-coupling methods, such as Kumada–Corriu, Suzuki–Miyaura, Ullmann reactions, have been carried out to optimize the experimental conditions in order to prepare the linear π-conjugated compounds with high yields. As can been seen

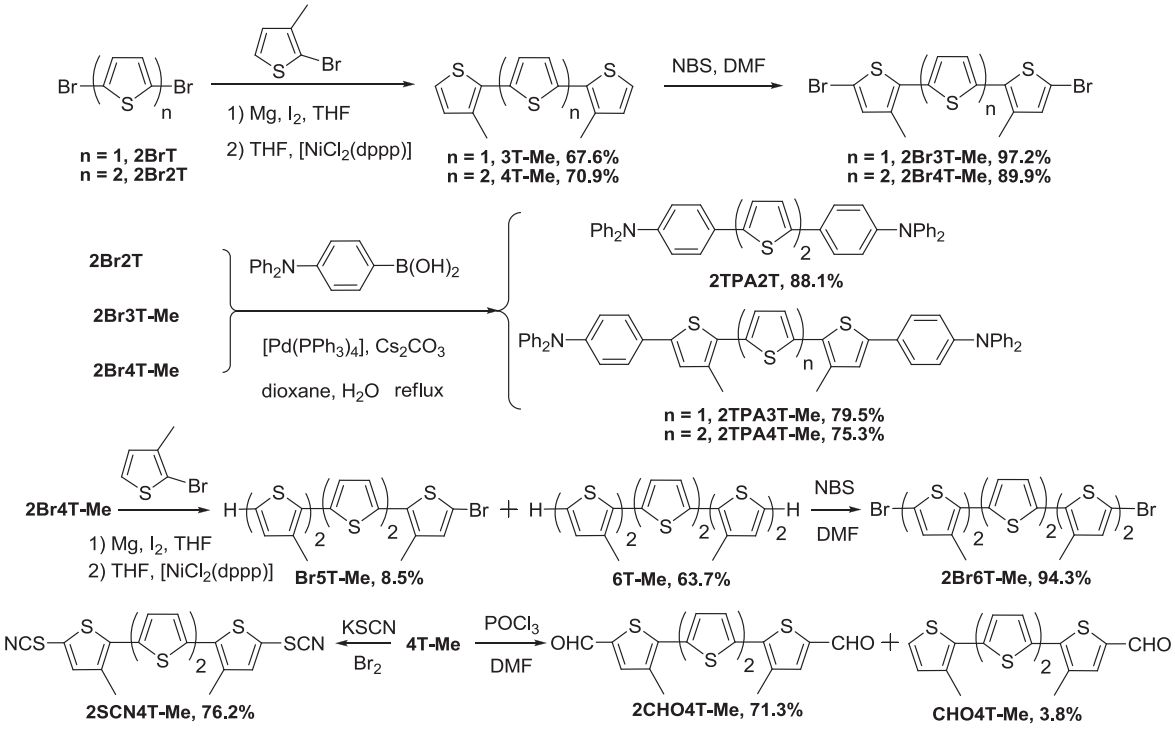

Scheme 1. Synthetic route of oligothiophene-based heterocyclic aromatic fluorescent compounds.

All these obtained linear heterocyclic aromatic compounds promote us to further explore possible rules between their structures and properties, for example, the relationship between the

in Figs. SI1–9, all the heterocyclic aromatic compounds have been characterized by ^{1}H, ^{13}C NMR, and EI-TOF-MS spectra, and the results clearly demonstrate the formation of expected compounds.

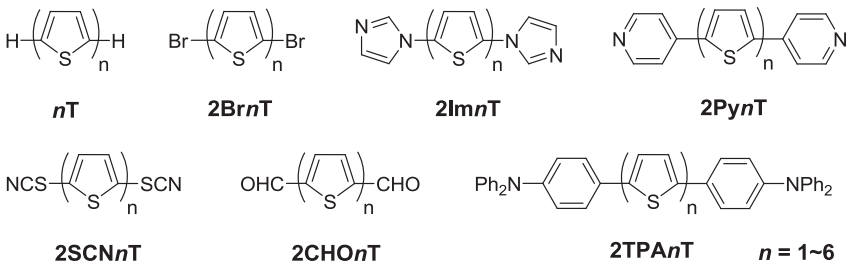

Scheme 2. Molecular structures of oligothiophene-based heterocyclic aromatic fluorescent compounds.

In comparison with the oligothiophenes bearing no substituent, we have previously demonstrated that the introduction of a β-methyl group to the thiophene ring can effectively increase the solubility of resulting compounds in organic solvents without impacting the molecular planarity and electronic structure, which facilitates the related C–C bond and C–N bond cross-coupling reactions and improves the final yields.[16c] In this work, β-methylthiophene extended quaterthiophene compounds **6T-Me** and **Br5T-Me** were firstly prepared in one-pot reaction (63.7 and 8.5%) by the treatment of Grignard reagents obtained from corresponding oligothiophene-based bromides and magnesium turnings with a [$NiCl_2$(dppp)] catalyst in dry THF. It is worth mentioning that **Br5T-Me** has been further confirmed by the $^1H-^1H$ correlation spectroscopy (COSY) NMR shown in Fig. SI5c.

As anticipated, triphenylamino-terminated compounds **2TPA2T**, **2TPA3T-Me**, and **2TPA4T-Me** were synthesized with satisfactory yields in the presence of a [$Pd(PPh_3)_4$] catalyst by using a strong cross-coupling reagent, i.e., 4-(diphenylamino) phenylboronic acid. Furthermore, the resultant yields for **2TPA2T**, **2TPA3T-Me**, and **2TPA4T-Me** can be improved by using Cs_2CO_3 instead of Na_2CO_3 as a base. As shown in Scheme 1, formyl terminated quaterthiophene compound **2CHO4T-Me** was also firstly prepared by the classical Vilsmeier–Haack reaction in a yield of 71.3%, in which the mono-formyl compound **CHO4T-Me** was carefully separated as a by-product in a yield of 3.8% by silica gel column chromatography.

As illustrated in Fig. 1, all new compounds show characteristic absorptions at 350–432 nm in their electronic spectra

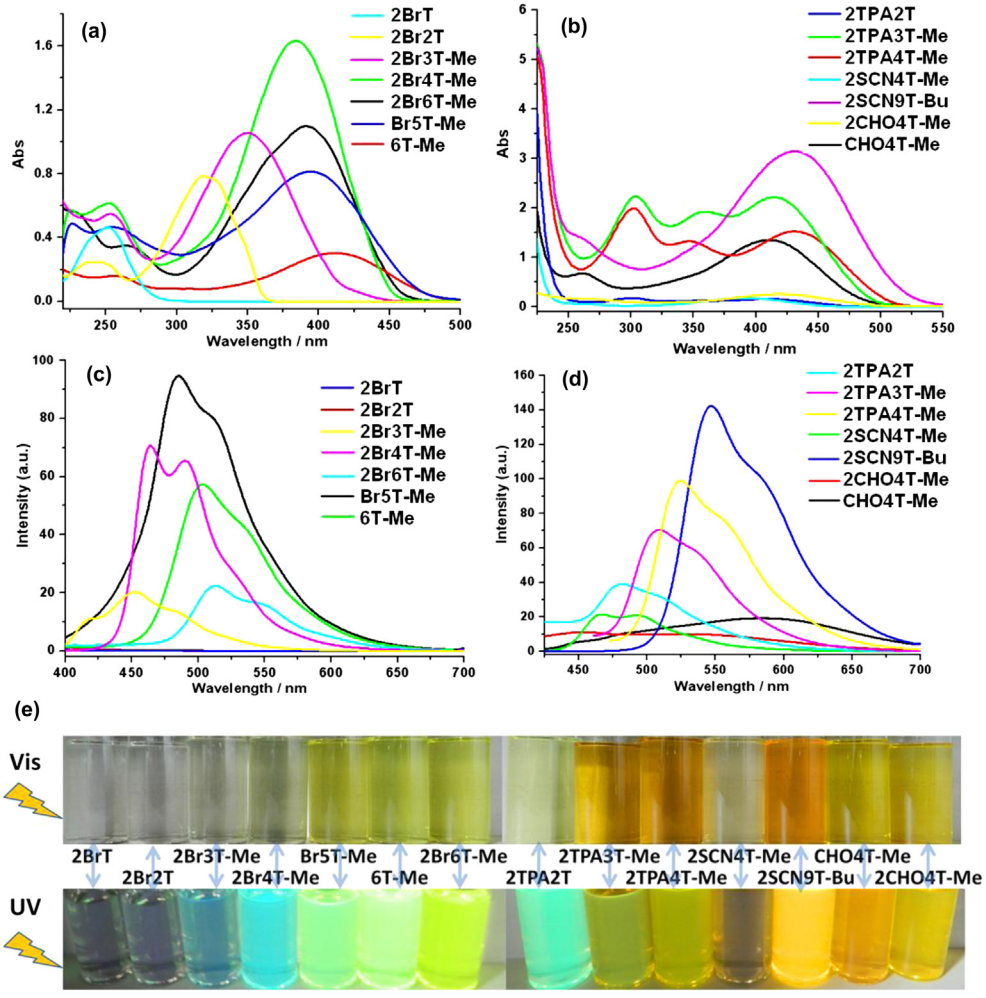

Fig. 1. UV–vis absorption spectra (a, b), fluorescence emission excited at 350 nm (c, d) and their visual photographs (e) for heterocyclic aromatic compounds in their methanol solutions at room temperature with the same concentration of 5.0×10^{-5} mol/L.

corresponding to the π–π* transitions within the conjugated system of the whole aromatic heterocycles. As expected, the maximum absorption wavelengths are shifted to lower energy bands when the number of aromatic heterocycles is increased, which are comparable with those in oligothiophene compounds. Moreover, it is noted that this family of linear heterocyclic aromatic compounds are fluorescence active, and compound **Br5T-Me** shows a yellow-green fluorescence peak at 485 nm and a UV–vis absorption peak at 395 nm (ε=16,300) simultaneously. Similar bathochromic shifts have been found in the fluorescence emission spectra of compounds **2SCN4T-Me**, **2SCN9T-Bu**, **2TPA2T**, **2TPA3T-Me**, and **2TPA4T-Me** when the number of aromatic heterocycles (namely delocalized π-systems) is increased. In contrast, compounds **CHO4T-Me** and **2CHO4T-Me** have the poor intensity of fluorescence emission because of the fluorescence quenching of formyl group. Compared with the 1,10-phenanthroline-based[16c] aromatic heterocyclic compounds showing blue fluorescence emissions, obvious red-shifts are observed for these oligothiophene-based compounds especially for those pyridyl and triphenylamino-terminated terthiophene and quaterthiophene compounds, where green fluorescence emissions are observed. The alterations of molecular rigidity, planarity, and electronic structures of oligothiophene-based compounds are suggested to be the main reason for the above-mentioned red-shifts in UV–vis absorption and fluorescence emission spectra.

2.2. Single-crystal structure of $(2TPA2T)_2\cdot(CH_3OH)$

X-ray single-crystal diffraction study for compound **2TPA2T** methanol semisolvate reveals that the two central thiophene rings are coplanar and they exhibit a trans configuration with the dihedral angle of 25.8(5)° between each central thiophene ring and its neighboring benzene ring of the triphenylamino unit, as depicted in Fig. 2. It is generally believed that increasing the planarity, which could reduce the reorganization energy and enhance the electronic coupling between adjacent molecules, would be much more efficient than distorted stacking for the transportation of charge carriers.[18]

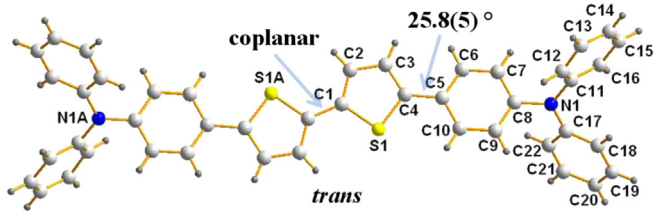

Fig. 2. An ORTEP diagram (30% thermal probability ellipsoids) of the molecular structure of **2TPA2T** showing the dihedral angles and relative configurations between adjacent aromatic heterocycles.

2.3. Thermal stability

Thermal durability has significant impact on the device performance, which is one of the most essential parameters for fine-tuned applications of the small organic molecules.[19] Twelve oligothiophene-based compounds have been checked herein in TGA measurements and a parameter of Td_{10} (10% weight-loss temperature) is used to describe the thermal stability of compounds. As shown in Fig. 3, TGA of oligothiophenes **2TPA2T**, **2TPA3T-Me**, **2TPA4T-Me**, **6T-Me**, **2Im3T-Me**, **2Im4T-Me**, **2Py3T-Me**, and **2Py4T-Me** indicates that they can keep unchangeable when the temperature is below 200 °C. The Td_{10} values for them range from 271 to 451 °C. Furthermore, quaterthiophene

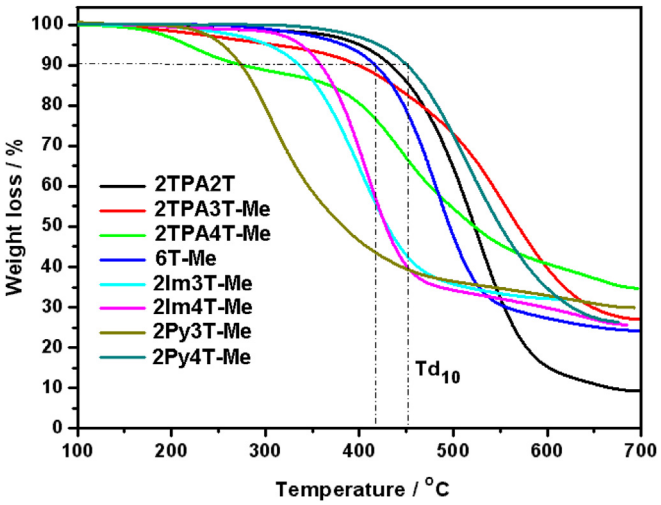

Fig. 3. TGA graphs of oligothiophene-based compounds **2TPA2T**, **2TPA3T-Me**, **2TPA4T-Me**, **6T-Me**, **2Im3T-Me**, **2Im4T-Me**, **2Py3T-Me**, and **2Py4T-Me**.

derivatives **2Im4T-Me**, **2Py4T-Me**, and **6T-Me** show more remarkable performance in the thermal stability compared with corresponding terthiophene-based counterparts. In contrast, the Td_{10} values for compounds **2TPA4T-Me**, **2Br6T-Me**, **2CHO4T-Me**, and **2SCN4T-Me** are found to be in the range 217–289 °C, indicative of lower thermal stability.

2.4. Electrochemical properties

The electrochemical behavior of heterocyclic aromatic compounds was examined by cyclic voltammetry (CV) and differential pulse voltammetry (DPV) in their 1.0×10^{-3} M CH_2Cl_2 solutions containing 0.1 M $TBAClO_4$ as the supporting electrolyte at different scan rates (10, 20, 50, 80, 100 mV s^{-1}) in Fig. 4. All potentials reported herein were calibrated with the ferrocene/ferrocenium couple (Fc^+/Fc) as internal standard. Oxidation onset potentials (E_{ox}^{onset}), as well as HOMO/LUMO energy levels were determined by a combined analysis of the CV, DPV and absorption data are summarized in Table 1. The onset oxidation was measured relative to the Fc^+/Fc couple for which an energy level of −5.10 eV versus vacuum was assumed.[20]

As depicted in Fig. 4 and SI11, TPA-terminated oligothiophenes show reversible and well-defined redox response in the CV measurements. The onset oxidation potentials (E_{ox}^{onset}) of these compounds were determined to be 0.05 V for **2TPA4T-Me**, 0.08 V for **2TPA3T-Me**, and 0.14 V for **2TPA2T**. In general, the HOMO of D–A oligomer is determined by the HOMO of the donor unit, while the LUMO of D–A oligomer is controlled by the LUMO of acceptor unit. As can be seen in Fig. 4, one or two oxidation waves have been observed for all compounds, and the reduction potentials as well as the measured currents are found to be dependent on their molecular structures. The first oxidation wave can be attributed to the formation of cation-radical species and the second one is ascribed to the successive oxidation of cation-radical to its corresponding dication, which have been observed previously in other oligothiophene systems.[20,21]

2.5. Density function theory (DFT) computations

DFT calculations are carried out with the Gaussian 03, Revision C.02 programs,[22] using the B3LYP method and 6-31G* basis set. The fixed atom coordinates of 42 oligothiophene-based compounds, based on the structural parameters determined by the

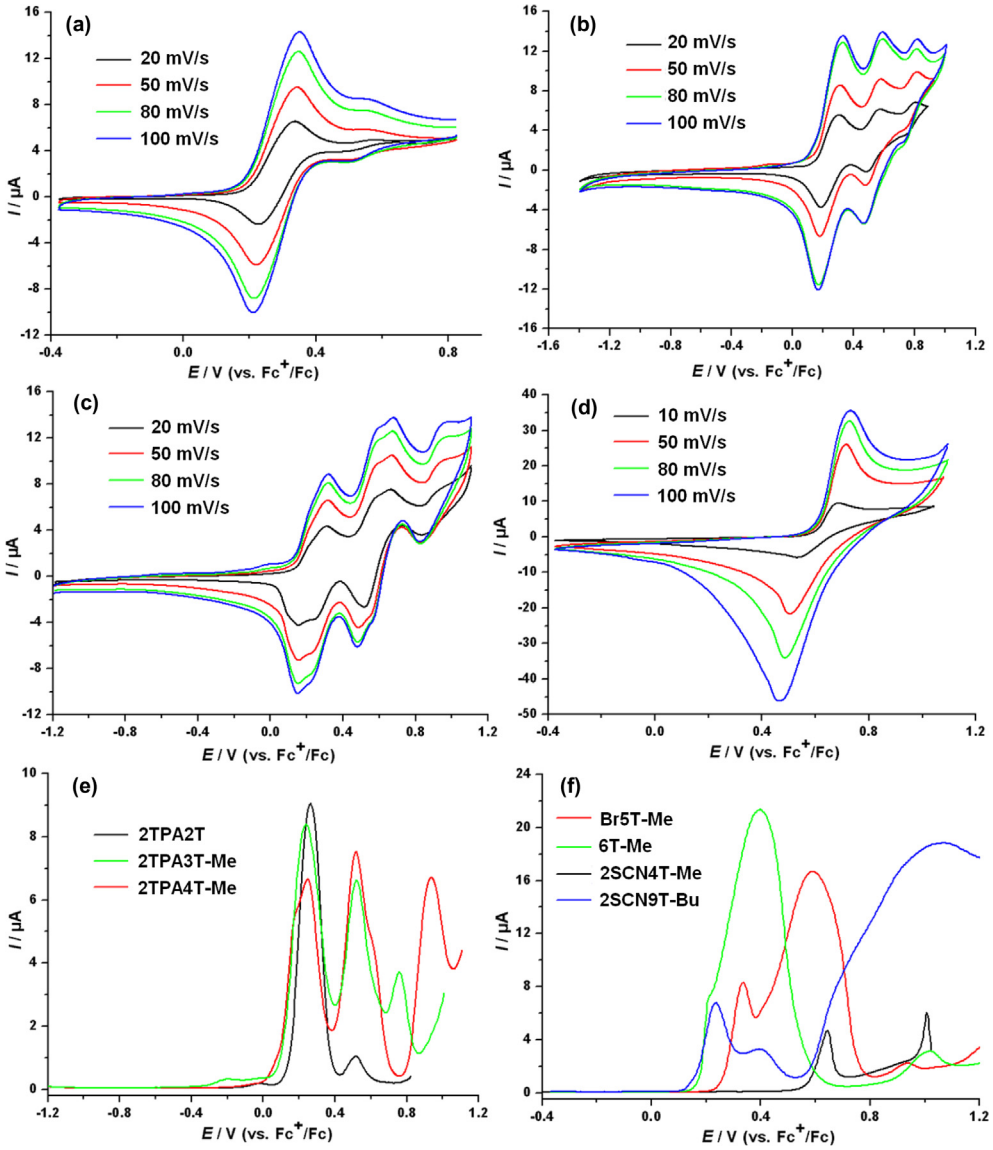

Fig. 4. CV (a, b, c, d) and DPV (e, f) for heterocyclic aromatic compounds in CH_2Cl_2 (1.0×10^{-3} M) containing 0.10 M of $TBAClO_4$ under argon. The different scanning rate: 10, 20, 50, 80, 100 mV/s (a) **2TPA2T**; (b) **2TPA3T-Me**; (c) **2TPA4T-Me**; (d) **2SCN4T-Me** versus Fc^+/Fc.

Table 1
UV–vis absorption and fluorescence emission data, optical, electrochemistry, and calculated HOMO–LUMO energy gaps (*Eg*) for related heterocyclic aromatic compounds

Compounds	UV–vis λ_{max} [nm (eV)]	ε (L mol^{-1} cm^{-1})	E_g^{opta} (eV)	E_g^{calcdb} (eV)	Fluorescence λ_{max} (nm)	Td_{10}[c] (°C)	E_{ox}^{onsetd} (V)	E_{HOMO}[e] (eV)	E_{LUMO}[f] (eV)
2TPA2T	409 (3.03)	3200	2.61	3.40	482	432	0.14	−5.24	−2.63
2TPA3T-Me	414 (2.99)	44,500	2.54	3.07	508	398	0.08	−5.18	−2.64
2Im3T-Me	357 (3.47)	47,700	2.96	3.45	460	335	0.35	−5.45	−2.49
2Py3T-Me	399 (3.11)	45,800	2.66	2.99	506	273	—	—	—
2TPA4T-Me	430 (2.88)	30,600	2.46	2.83	525	271	0.05	−5.15	−2.69
2Im4T-Me	389 (3.19)	57,700	2.73	3.02	452	358	—	—	—
2Py4T-Me	420 (2.95)	27,800	2.54	2.80	533	451	0.30	−5.40	−2.86
2CHO4T-Me	419 (2.96)	5100	2.47	2.78	454	217	—	—	—
CHO4T-Me	410 (3.02)	27,100	2.54	2.83	584	—	—	—	—
2Br4T-Me	384 (3.23)	32,700	2.79	3.21	482	—	—	—	—
2SCN4T-Me	390 (3.18)	3580	2.71	2.97	468	289	0.55	−5.65	−2.94
2SCN9T-Bu	432 (2.87)	62,900	2.39	2.50	547	—	0.14	−5.24	−2.85
Br5T-Me	395 (3.14)	16,300	2.64	2.83	485	278	0.25	−5.35	−2.71
6T-Me	411 (3.02)	6060	2.57	2.67	503	417	0.18	−5.28	−2.71
2Br6T-Me	392 (3.16)	22,000	2.74	2.61	513	220	—	—	—

[a] Optical band gap determined from the UV–vis absorptions in their methanol solutions.
[b] The geometries are calculated by B3LYP method and 6-31G* basis set.
[c] 10% Weight-loss temperature.
[d] Oxidation onset potentials determined from DPV versus Fc^+/Fc.
[e] Calculated from $E_{HOMO}=-(E_{ox}^{onset}+5.10)$.
[f] Calculated from $E_{LUMO}=E_{HOMO}+E_g^{opt}$.

X-ray diffraction method and fully optimization, are used for the highest occupied molecular orbital (HOMO) and the lowest unoccupied molecular orbital (LUMO) gap calculations (Table 1). The resultant HOMO–LUMO gaps for TPA-extended compounds **2TPA2T**, **2TPA3T-Me**, and **2TPA4T-Me** are 3.40, 3.07, and 2.83 eV, respectively, which are analogous to their UV–vis absorption peaks.

According to the DPV measurements, the corresponding oxidation potentials for four quaterthiophene-based derivatives **2SCN4T-Me**, **2Py4T-Me,**[16c] **2TPA4T-Me**, and **6T-Me** were determined to be 0.55, 0.30, 0.05, and 0.18 V, respectively (Table 1, Fig. 4e and f). Further analyses of the frontier orbitals reveal that the introduction of electron-donating groups raises the HOMO energy levels, while the introduction of electron-withdrawing groups lowers the LUMO energy levels, which will greatly decrease the HOMO–LUMO gaps of resultant compounds. It is noted that there is an almost linear relationship between the experimentally determined (CV and UV–vis absorption spectra) and the theoretically calculated energy levels for the HOMOs and LUMOs of these triphenylamino- and thiocyano-terminated oligothiophene hybrids (Figs. 5 and 6). This relationship demonstrates that, despite the uncertainty in the calculated absolute values, theoretical calculations can serve as a useful tool to predict and guide the synthesis of future oligomer and polymer materials at least in some cases.

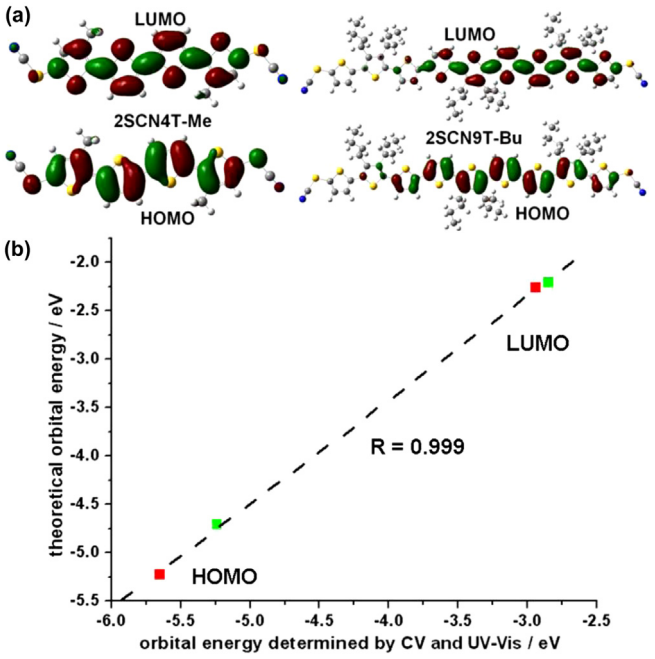

Fig. 6. (a) HOMO (bottom) and LUMO (top) of **2SCN4T-Me** (left) and **2SCN9T-Bu** (right) calculated with B3LYP/6-31G*. (b) Energy level correlation between CV and computational data; *Y*-axis: **2SCN4T-Me** (red) and **2SCN9T-Bu** (green).

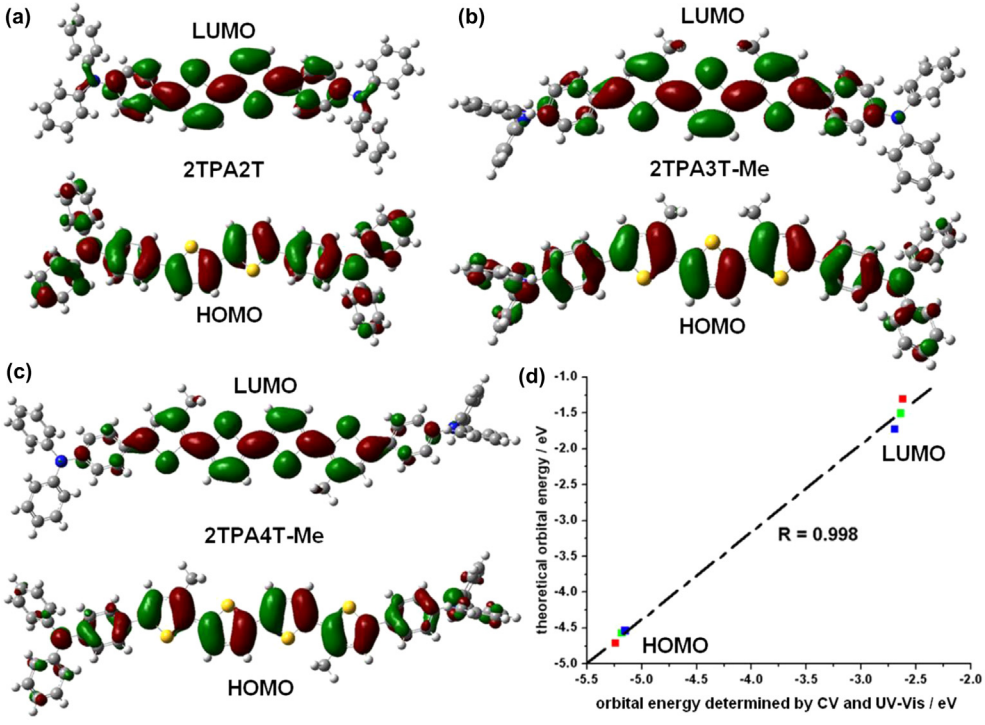

Fig. 5. HOMOs and LUMOs of **2TPA2T** (a), **2TPA3T-Me** (b), and **2TPA4T-Me** (c) calculated with B3LYP/6-31G*. (d) Energy level correlation between CV, UV–vis absorption spectra, and computational data; *Y*-axis: **2TPA2T** (red), **2TPA3T-Me** (green), **2TPA4T-Me** (blue).

To make further comparisons of the HOMO–LUMO gaps from a theoretical and experimental perspective, the extrapolation for a series of π-conjugated oligothiophenes at the B3LYP/6-31G* level was carried out. However, the theoretical prediction is not accurate in accordance with the experimental results. To solve this problem, Zade et al.[10] used the correction index method where the relationship between the first adiabatic ionization potential of oligothiophenes and chain length correlates linearly with an empirically obtained value of $1/(n^{0.75})$. The same correction strategy has been used herein, but a new thienyl ring coefficient (n_{corr}) has been introduced (Eq. 1) to correct the effective number of oligothiophene (n_{eff}) according to Kuhn's equation[23] (see SI) due to the presence of different terminal groups. So the n_{eff} coefficient includes the contribution of different terminal groups in our

compounds, which leads to better correlation of linear fitting. For example, the prediction of HOMO–LUMO gap for a nonathiophene compound **2SCN9T-Bu** is 2.63 eV from the curve without corrected (Fig. SI17c, $Y=2.22X+2.38$), while the prediction value is 2.45 eV with the n_{eff} coefficient correction (Fig. SI17d, $Y=4.41X+2.00$). Compared where the optical band gap and HOMO–LUMO gap for **2SCN9T-Bu** ($E_g^{\text{opt}}=2.39$ and $E_g^{\text{calcd}}=2.50$ eV),[17] it is suggested that the introduction of the n_{eff} coefficient can help to predict more accurately the HOMO–LUMO gaps of various D–A spacer functionalized oligothiophene systems. Similar results have been obtained for all the oligothiophene-based compounds with different end-capped groups, as can be seen in Fig. SI17.

$$Y = A/n_{\text{eff}} + B \tag{1}$$

$$n_{\text{eff}} = n + n_{\text{corr}} \tag{2}$$

On the one hand, by introducing a parameter of n_{corr}, the convergence behavior shows not only better correlation of linear fitting, but also more precise theoretical prediction of band gap for oligomers and polymers. Actually, another important question is whether the corrected value is reasonable. We believe the answer is yes at least for polythiophenes because the limitation of band gap is around 2.00 eV based on the extrapolation of HOMO–LUMO gaps (see Fig. SI17). On the other hand, these parameters can assist us to evaluate the effects of different D–A terminal groups from the quantitative viewpoint. As illustrated in Fig. 7, the contour diagrams of compounds mentioned in this work have the traits of visualizing, intuition, and easy understanding, which can guide us to rationally design the HOMO and LUMO energy levels and finely tune the band gaps for these oligothiophene-based compounds. More importantly, this method can help us to find some potentially useful materials with required band gaps and suitable energy levels more easily, hence improving our ways of working and reducing drastically the research time.

Based upon the above-mentioned electronic spectra, electrochemistry, and DFT computational data, systematic comparisons in terms of the band-gap engineering show that the energy discrepancy between the HOMO and LUMO decreases as the length of conjugation increases. However, when the number of monomer units exceeds a certain value at which the effective conjugation length is saturated, the band gap starts to level off. Therefore, unlimited extension of the conjugation length results only in a limited reduction of the band gap. Moreover, incorporation of the electron-donating or electron-withdrawing substituents directly into the aromatic unit in the main chain represents another effective way to finely tune the electronic structure by perturbing the molecular orbitals through either inductive or mesomeric effects. We think our effects on studying the functionalized oligothiophene-based heterocyclic aromatic fluorescent compounds with various D–A spacers and adjustable electronic properties can provide a theoretical screening approach for the discovery of novel organic semiconductor cores and terminals before conventional chemical synthesis.

3. Conclusions

Following the idea of introducing specific organic D–A hybrids to promote the direct electronic separation and transportation and retaining the effective and linear delocalized π systems simultaneously, a series of linear oligothiophene-based heterocyclic aromatic fluorescent compounds with molecular lengths more than 2 nm (**2TPA2T**, **2TPA3T-Me**, **2TPA4T-Me**, **2SCN4T-Me**, **2SCN9T-Bu**, **2CHO4T-Me**, **CHO4T-Me**, **6T-Me**, **Br5T**, and **2Br6T**) have been reported in this work. Synthetic, structural, thermal, computational,

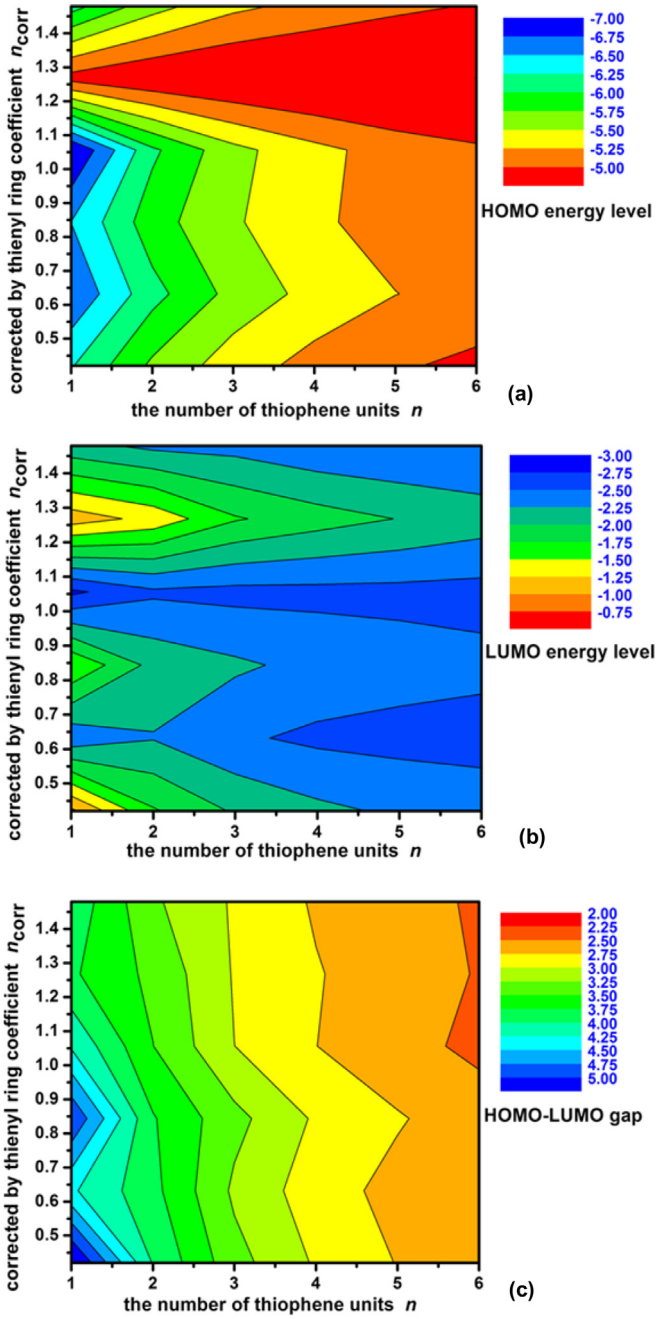

Fig. 7. Contour diagrams of HOMO (a), LUMO (b) energy level, and HOMO–LUMO gap (c) for 42 oligothiophene-based compounds calculated with B3LYP/6-31G*.

and spectral comparisons have been carried out for these mono- and bi-β-methylthiophene/thiocyanato/triphenylamino/formyl extended oligothiophene compounds with different number of aromatic heterocycles in order to reveal the differences between cross-coupling approaches and experimental conditions on the C–C bond and C–N bond formation, molecular conformation, and dihedral angles between neighboring heterocycles, band gaps and energy levels, electronic, fluorescent, and electrochemistry spectra of related compounds. X-ray single-crystal structure of **2TPA2T** methanol semisolvate reveals a trans configuration with different dihedral angles between adjacent aromatic heterocycles. Compounds **2TPA2T**, **2Py4T-Me**, and **6T-Me** show excellent performance in the thermal stability, which suggests that they may be good candidates for the device fabrication.

A theoretical and experimental perspective has been carried out for this family of linear oligothiophene-based heterocyclic aromatic fluorescent compounds, which have effective π-conjugated systems with D–π–D or A–π–A structures and different terminal groups namely, bromo, imidazolyl, pyridyl, thiocyano, formyl, and triphenylamino tails. The influences of introducing different D–A functionalized tails on the band-gap convergence have also been discussed, where the convergence behavior corrected via the thienyl ring coefficient shows better correlation of linear fitting based on the extrapolation of HOMO–LUMO gaps. As we know, designing better organic optoelectronic materials requires a comprehensive understanding of the electronic structure. A theoretical screening and optimizing approach can help us find novel organic semiconductors as soon and as effectively as possible prior to the chemical synthesis. We hope this study can provide some useful information on the general rules between structures and properties. Further studies are being undertaken on the field-effect, light-emitting, photoresponsive, and photovoltaic properties of these linear aromatic heterocycle-based nanowires, nanocomposite films, and nanodevices.

4. Experimental section

4.1. General

All melting points were measured without any corrections. Unless otherwise specified, solvent of analytical grade was purchased directly from commercial sources and used without any further purification. Tetrahydrofuran (THF) was freshly distilled from the sodium/benzophenone mixture prior to use. Anhydrous solvents were drawn into syringes under the flow of dry N_2 gas and directly transferred into the reaction flasks to avoid contamination. Column chromatography was carried out on silica gel (300–400 mesh) and analytical thin-layer chromatography (TLC) was performed on glass plates of silica gel GF-254 with detection by UV. Standard techniques for synthesis were carried out under argon atmosphere. Heterocyclic aromatic compounds 3,3″-dimethyl-2,2′:5′,2″-terthiophene (**3T-Me**), 5,5″-dibromo-3,3″-dimethyl-2,2′:5′,2″-terthiophene (**2Br3T-Me**), 3,3‴-dimethyl-2,2′:5′,2″:5″,2‴-quaterthiophene (**4T-Me**), and 5,5‴-dibromo-3,3‴-dimethyl-2,2′:5′,2″:5″,2‴-quaterthiophene (**2Br4T-Me**) were prepared from 2,5-dibromothiophene (**2BrT**) and 5,5′-dibromo-2,2′-bithiophene (**2Br2T**) via literature methods.[16c]

4.2. Syntheses and characterizations of heterocyclic aromatic compounds

4.2.1. ***2TPA2T***. A mixture of **2Br2T** (0.32 g, 1.00 mmol), 4-(diphenylamino)phenylboronic acid (1.16 g, 4.00 mmol), cesium carbonate (1.30 g, 4.00 mmol), $[Pd(PPh_3)_4]$ (0.06 g, 0.05 mmol), toluene (20 mL), and water (5 mL) was degassed for 0.5 h and heated to reflux for 40 h under argon atmosphere. The mixture was then allowed to cool to the room temperature and extracted with chloroform. The resulting organic layer was dried over anhydrous sodium sulfate and filtered. The filtrate was evaporated, and the residue was purified by column chromatography over silica gel using hexane and dichloromethane (1:1) as eluent to give 0.57 g (88.1%) of **2TPA2T** as a yellow solid. The yellow single crystals of **2TPA2T** suitable for X-ray diffraction measurement were grown and isolated from DMF by slow evaporation in air at room temperature for 2 weeks. Melting point: >300 °C. Anal. Calcd for $[C_{44}H_{32}N_2S_2]$: C, 80.95; H, 4.94; N, 4.29%. Found: C, 80.71; H, 5.12; N, 4.13%. Main FTIR absorptions (KBr pellets, cm^{-1}): 3450 (b), 2361 (m), 1590 (s), 1490 (vs), 1327 (m), 1283 (s), 1183 (w), 1070 (w), 830 (w), 796 (w), 757 (m), 694 (m), 512 (w). ^1H NMR (500 MHz, $CDCl_3$) δ: 7.46 (d, 4H, J=8.5 Hz, ph), 7.28 (t, 8H, ph), 7.13 (d, 12H=8H+4H, J=7.5 Hz, ph+thio), 7.07 (d, 4H, J=8.3 Hz, ph), 7.04 (t, 4H, ph). ^{13}C NMR (125 MHz, $CDCl_3$) δ: 147.5, 147.4, 142.9, 136.0, 129.3, 128.1, 126.4, 124.6, 124.3, 123.6, 123.2, 122.9. EI-TOF-MS (m/z): calcd for $[C_{44}H_{32}N_2S_2]^+$: 652.2 (100.0%), 653.2 (49.9%). Found: 652.0 (100.0%), 653.0 (11.6%).

4.2.2. ***2TPA3T-Me***. The synthesis of **2TPA3T-Me** was similar to that described for **2TPA2T**. Yield: 79.5% (0.61 g) as an orange solid. Melting point: >300 °C. Anal. Calcd for $[C_{50}H_{38}N_2S_3]$: C, 78.70; H, 5.02; N, 3.67%. Found: C, 78.58; H, 5.12; N, 3.55%. Main FTIR absorptions (KBr pellets, cm^{-1}): 3457 (b), 2365 (m), 1587 (s), 1494 (vs), 1324 (m), 1273 (s), 1175 (w), 1087 (m), 1025 (m), 813 (m), 749 (m), 694 (m), 509 (w). ^1H NMR (500 MHz, $CDCl_3$) δ: 7.45 (d, 4H, J=8.0 Hz, ph), 7.29 (t, 8H, ph), 7.14 (d, 8H, J=8.0 Hz, ph), 7.11 (m, 4H, thio), 7.05 (m, 8H, ph), 2.43 (s, 6H, CH_3). ^{13}C NMR (125 MHz, $CDCl_3$) δ: 146.7, 141.4, 134.7, 129.3, 124.6, 124.3, 124.2, 124.1, 123.6, 123.1, 122.8, 122.7, 15.9. EI-TOF-MS (m/z): calcd for $[C_{50}H_{38}N_2S_3]^+$: 762.2 (100.0%), 763.2 (57.2%), 764.2 (15.3%). Found: 762.1 (100.0%), 763.2 (38.1%), 764.2 (6.7%).

4.2.3. ***2TPA4T-Me***. The synthesis of **2TPA4T-Me** was similar to that described for **2TPA2T**. Yield: 75.3% (0.64 g) as a red solid. Melting point: 219–221 °C. Anal. Calcd for $[C_{54}H_{40}N_2S_4]$: C, 76.74; H, 4.77; N, 3.31%. Found: C, 76.52; H, 4.93; N, 3.15%. Main FTIR absorptions (KBr pellets, cm^{-1}): 3451 (b), 2359 (m), 1587 (s), 1489 (vs), 1324 (m), 1267 (s), 1092 (s), 1020 (s), 798 (s), 757 (m), 695 (s), 618 (w), 510 (w). ^1H NMR (500 MHz, $CDCl_3$) δ: 7.45 (d, 4H, J=8.6 Hz, ph), 7.27 (t, 8H, ph), 7.14 (d, 12H, J=7.65 Hz, ph+thio), 7.05 (m, 10H, ph+thio), 2.44 (s, 6H, CH_3). ^{13}C NMR (125 MHz, $CDCl_3$) δ: 147.4, 141.5, 135.0, 129.3, 125.6, 124.6, 124.3, 124.1, 123.9, 123.5, 123.2, 122.8, 15.9. EI-TOF-MS (m/z): calcd for $[C_{54}H_{40}N_2S_4]^+$: 844.2 (100.0%), 845.2 (62.1%), 846.2 (19.1%). Found: 844.2 (100.0%), 845.2 (32.4%), 846.2 (8.9%).

4.2.4. ***6T-Me*** *and* ***Br5T-Me***. Activated Mg turnings (1.04 g, 42.95 mmol) in 20 mL of anhydrous THF and a catalytic amount of iodine were added to a flame-dried 50 mL three-neck flask equipped with vigorous stirring at the room temperature under argon atmosphere. Then a solution of 2-bromo-3-methylthiophene (2.5 mL, 22.20 mmol) in 10 mL of anhydrous THF was slowly dropped into the reaction mixture. Once the vigorous reaction had started, the rest of the 2-bromo-3-methylthiophene solution was added dropwise to keep the mixture refluxing over 20 min. The reaction mixture was allowed to proceed for 2 h at the room temperature and cannulated into an ice-cooled solution of **2Br4T-Me** (2.58 g, 5.00 mmol) and $[Ni(dppp)Cl_2]$ (0.11 g, 0.20 mmol) in dry THF (40 mL). After being stirred for 2 h at the room temperature, the reaction mixture was refluxed for another 12 h and then cooled to the room temperature. The reaction mixture was quenched with saturated NH_4Cl aqueous solution, extracted thoroughly with chloroform ($CHCl_3$) until no more products could be detected by TLC, washed with brine. The resulting organic layer was dried over anhydrous sodium sulfate and filtered. Compounds **6T-Me** and **Br5T-Me** were purified by silica gel column chromatography employing $CHCl_3$ solution to give red solid in yields of 1.75 g (63.7%) for **6T-Me** and 0.23 g (8.5%) for **Br5T-Me**, respectively. Compound **6T-Me**: Melting point: >300 °C. Anal. Calcd for $[C_{28}H_{22}S_6]$: C, 61.05; H, 4.03%. Found: C, 60.87; H, 4.21%. Main FTIR absorptions (KBr pellets, cm^{-1}): 3408 (b), 2920 (s), 2854 (m), 1446 (vs), 1062 (m), 1022 (m), 823 (s), 779 (s), 709 (s), 615 (m). ^1H NMR (500 MHz, $CDCl_3$) δ: 7.14 (d, 4H, J=4.6 Hz, thio), 7.07 (d, 2H, J=3.2 Hz, thio), 6.94 (s, 2H, thio), 6.88 (d, 2H, J=5.0 Hz, thio), 2.44 (d, 12H, J=5.4 Hz, CH_3). ^{13}C NMR (125 MHz, $CDCl_3$) δ: 136.3, 135.2, 134.4, 134.2, 134.0, 131.5, 130.2, 129.5, 125.8, 123.9, 123.3, 29.5, 29.2, 15.6, 15.4. EI-TOF-MS (m/z): calcd for $[C_{28}H_{22}S_6]^+$: 550.0 (100.0%), 551.0 (30.5%), 552.0 (27.2%). Found: 549.8 (100.0%), 550.9 (52.8%), 551.9 (12.2%).

Compound **Br5T-Me**: Melting point: >300 °C. Anal. Calcd for [$C_{23}H_{17}BrS_5$]: C, 51.77; H, 3.21%. Found: C, 51.55; H, 3.43%. Main FTIR absorptions (KBr pellets, cm^{-1}): 3409 (b), 2922 (s), 2362 (w), 1730 (m), 1448 (s), 1062 (s), 788 (s), 710 (m), 618 (m). ^1H NMR (500 MHz, $CDCl_3$) δ: 7.14 (d, 2H, J=3.4 Hz, thio), 7.12 (d, 1H, J=3.0 Hz, thio), 7.07 (d, 1H, J=2.8 Hz, thio), 6.99 (d, 1H, J=2.8 Hz, thio), 6.93 (s, 1H, thio), 6.88 (d, 1H, J=4.9 Hz, thio), 6.86 (s, 1H, thio), 2.43 (d, 6H, J=3.4 Hz, CH_3), 2.37 (s, 3H, CH_3). ^{13}C NMR (125 MHz, $CDCl_3$) δ: 137.1, 135.7, 134.5, 134.2, 134.0, 132.4, 131.6, 130.4, 129.7, 126.5, 125.9, 124.1, 123.8, 123.3, 110.1, 15.7, 15.5, 15.4. EI-TOF-MS (m/z): calcd for $[C_{23}H_{17}BrS_5]^+$: 533.9 (100.0%), 531.9 (82.7%), 534.9 (28.5%), 532.9 (20.7%). Found: 533.9 (100.0%), 531.9 (97.2%), 534.9 (7.5%), 532.9 (9.6%).

4.2.5. ***2Br6T-Me***. In the absence of light, NBS (0.39 g, 2.20 mmol) was dissolved in DMF (5 mL) and injected into a solution of **6T-Me** (0.55 g, 1.00 mmol) in DMF (20 mL) at 40 °C under argon atmosphere. The mixture was stirred for 4 h at 60 °C and then cooled to the room temperature. Water (50 mL) was added into the mixture, and the crude yellow solid was precipitated, filtered, and rinsed with a 50% ethanol/water solution. The desired compound **2Br6T-Me** was purified by silica gel column chromatography ($CHCl_3$) to give red solid in yields of 0.67 g (94.3%). Melting point: >300 °C. Anal. Calcd for [$C_{28}H_{20}Br_2S_6$]: C, 47.46; H, 2.84%. Found: C, 47.22; H, 3.02%. Main FTIR absorptions (KBr pellets, cm^{-1}): 3406 (b), 2922 (s), 2854 (m), 1500 (m), 1446 (s), 1071 (m), 1018 (m), 829 (s), 788 (vs), 612 (m), 460 (m). ^1H NMR (500 MHz, $CDCl_3$) δ: 7.15 (d, 2H, J=3.1 Hz, thio), 7.07 (d, 2H, J=3.9 Hz, thio), 6.87 (d, 4H, J=9.4 Hz, thio), 2.43 (s, 6H, CH_3), 2.36 (s, 6H, CH_3). EI-TOF-MS (m/z): calcd for $[C_{28}H_{20}Br_2S_6]^+$: 707.8 (100.0%), 709.8 (68.1%), 705.8 (45.1%), 708.8 (26.9%). Found: 707.8 (100.0%), 709.8 (30.7%), 705.8 (21.6%), 708.8 (11.2%).

4.2.6. ***2SCN4T-Me***. A solution of compound **4T-Me** (0.66 g, 1.85 mmol) in $CHCl_3$ (15 mL) was added dropwise to a mixture of KSCN (10.90 g, 112.15 mmol) in methanol (30 mL) and Br_2 (2.9 mL, 56.62 mmol) in $CHCl_3$ (10 mL) at −78 °C. This mixture was stirred for 4 h at the room temperature, quenched with water, extracted with $CHCl_3$, and dried by anhydrous sodium sulfate. The solvent was removed by a rotatory evaporator and the residue was purified by silica gel column chromatography ($CHCl_3$). A red powder was obtained in a yield of 0.67 g (76.2%) after recrystallization from $CHCl_3$/*n*-hexane. Melting point: 275–278 °C. Anal. Calcd for [$C_{20}H_{12}N_2S_6$]: C, 50.82; H, 2.56; N, 5.93%. Found: C, 50.64; H, 2.82; N, 5.75%. Main FTIR absorptions (KBr pellets, cm^{-1}): 3449 (b), 2359 (m), 2152 (m), 1644 (s), 1582 (m), 1438 (s), 1400 (m), 1099 (s), 986 (m), 855 (m), 780 (s). ^1H NMR (500 MHz, $CDCl_3$) δ: 7.22 (s, 2H, thio), 7.18 (d, 2H, J=3.3 Hz, thio), 7.11 (d, 2H, J=3.6 Hz, thio), 2.41 (s, 6H, CH_3). ^{13}C NMR (125 MHz, $CDCl_3$) δ: 141.5, 135.3, 133.9, 127.6, 124.6, 115.2, 110.2, 15.5. EI-TOF-MS (m/z): calcd for $[C_{20}H_{12}N_2S_6]^+$: 471.9 (100.0%), 473.9 (27.4%), 472.9 (21.8%). Found: 471.9 (100.0%), 472.9 (4.5%), 473.9 (2.7%).

4.2.7. ***2CHO4T-Me*** *and* ***CHO4T-Me***. To a three-necked round bottom flask were added **4T-Me** (1.79 g, 5.00 mmol), 7.7 mL (100.00 mmol) of anhydrous DMF, and 40 mL of anhydrous chloroform. The solution was cooled to 0 °C, and 9.3 mL of $POCl_3$ (100.00 mmol) was added dropwise with stirring. The solution was then warmed to room temperature followed by refluxing for 4 h, then cooled to room temperature and poured into ice water. The water layer was extracted with dichloromethane (3×50 mL), and the organic layers were combined, washed with water (2×50 mL) and saturated aqueous sodium bicarbonate (2×50 mL), and then dried by anhydrous sodium sulfate. After evaporation of the solvent, compounds **2CHO4T-Me** and **CHO4T-Me** were purified by silica gel column chromatography ($CHCl_3$) to give red solid in yields of 1.48 g (71.3%) for **2CHO4T-Me** and 0.07 g (3.8%) for **CHO4T-Me**, respectively. Compound **2CHO4T-Me**: Melting point: 208–210 °C. Anal. Calcd for [$C_{20}H_{14}O_2S_4$]: C, 57.94; H, 3.40%. Found: C, 57.78; H, 3.62%. Main FTIR absorptions (KBr pellets, cm^{-1}): 3406 (vs), 2950 (m), 2212 (m), 1708 (m), 1581 (vs), 1350 (s), 1168 (m), 790 (m). ^1H NMR (500 MHz, $CDCl_3$) δ: 9.83 (s, 2H, CHO), 7.56 (s, 2H, thio), 7.27 (d, 2H, J=3.8 Hz, thio), 7.24 (d, 2H, J=3.8 Hz, thio), 2.50 (s, 6H, CH_3). ^{13}C NMR (125 MHz, $CDCl_3$) δ: 182.4, 140.4, 139.9, 138.2, 135.0, 134.9, 128.1, 124.8, 29.6, 15.9. EI-TOF-MS (m/z): calcd for $[C_{20}H_{14}O_2S_4]^+$: 414.0 (100.0%), 415.0 (25.1%). Found: 413.9 (100.0%), 414.9 (1.46%). Compound **CHO4T-Me**: Melting point: 170–172 °C. Anal. Calcd for [$C_{19}H_{14}OS_4$]: C, 59.03; H, 3.65%. Found: C, 58.85; H, 3.83%. Main FTIR absorptions (KBr pellets, cm^{-1}): 3446 (b), 1708 (m), 1657 (s), 1446 (m), 1377 (m), 1238 (m), 1184 (m), 1079 (w), 858 (w), 789 (m), 679 (m), 471 (w). ^1H NMR (500 MHz, $CDCl_3$) δ: 9.82 (s, 1H, CHO), 7.55 (s, 1H, thio), 7.25 (d, 1H, J=4.1 Hz, thio), 7.18 (m, 3H, thio), 7.07 (d, 1H, J=3.6 Hz, thio), 6.91 (d, 1H, J=5.0 Hz, thio), 2.49 (s, 3H, CH_3), 2.44 (s, 3H, CH_3). ^{13}C NMR (125 MHz, $CDCl_3$) δ: 182.4, 141.5, 140.4, 139.7, 139.1, 136.6, 135.8, 134.7, 134.4, 134.1, 131.6, 128.1, 126.2, 124.6, 124.1, 123.7, 29.7, 15.9, 15.5. EI-TOF-MS (m/z): calcd for $[C_{22}H_{16}N_2S_2]^+$: 386.6. Found: 386.0.

4.3. X-ray data collection and structural determination

Single-crystal sample of **2TPA2T** methanol semisolvate was covered with glue and mounted on a glass fiber and then used for data collection. Crystallographic data were collected on a Bruker SMART 1K CCD diffractometer, using graphite mono-chromated Mo Kα radiation (λ=0.71073 Å). The crystal system was determined by Laue symmetry and the space group was assigned on the basis of systematic absences using XPREP.[24] Absorption corrections were performed to all data and the structure was solved by direct methods and refined by full-matrix least-squares method on F^2_{obs} by using the SHELXTL-PC software package.[25] All non-H atoms were anisotropically refined and all hydrogen atoms were inserted in the calculated positions assigned fixed isotropic thermal parameters and allowed to ride on their respective parent atoms. The summary of the crystal data, experimental details, and refinement results is listed in Table SI1, whereas bond distances and angles are given in Table SI2.

Acknowledgements

This work was supported by the Major State Basic Research Development Programs (Nos. 2013CB922101 and 2011CB933300), the National Natural Science Foundation of China (Nos. 21171088 and 21021062) and Qing Lan Project.

Supplementary data

Tables of the crystal data, experimental details and refinement results, selected bond lengths and angles, figures of π–π stacking interactions, DFT computational details, ^1H, ^{13}C, ^1H–^1H COSY NMR and EI-TOF-MS spectra, and electrochemistry diagrams for related compounds are included. Supplementary data associated with this article can be found in the online version, at http://dx.doi.org/10.1016/j.tet.2013.06.087.

References and notes

1. For reviews, see: (a) Roncali, J. *Chem. Rev.* **1997**, *97*, 173–205; (b) Mishra, A.; Ma, C. Q.; Bauerle, P. *Chem. Rev.* **2009**, *109*, 1141–1276; (c) Liu, H. B.; Xu, J. L.; Li, Y. J.; Li, Y. L. *Acc. Chem. Res.* **2010**, *43*, 1496–1508.
2. Selected examples: (a) Fang, Z.; Eshbaugh, A. A.; Schanze, K. S. *J. Am. Chem. Soc.* **2011**, *133*, 3063–3069; (b) Mishra, A.; Pootrakulchote, N.; Wang, M. K.; Moon, S. J.; Zakeeruddin, S. M.; Graetzel, M.; Bauerle, P. *Adv. Funct. Mater.* **2011**, *21*, 963–970; (c) Scrascia, A.; Pastore, M.; Yin, L. X.; Picca, R. A.; Manca, M.; Guo, Y.

C.; De Angelis, F.; Della Sala, F.; Cingolani, R.; Gigli, G.; Ciccarella, G. *Curr. Org. Chem.* **2011**, *15*, 3535–3543; (d) Cheng, X. B.; Liang, M.; Sun, S. Y.; Shi, Y. B.; Ma, Z. J.; Sun, Z.; Xue, S. *Tetrahedron* **2012**, *68*, 5375–5385.
3. Selected examples: (a) Ku, S. Y.; Lyman, C. D.; Burke, D. J.; Treat, N. D.; Cochran, J. E.; Amir, E.; Perez, L. A.; Chabinyc, M. L.; Hawker, C. J. *Macromolecules* **2011**, *44*, 9533–9538; (b) Jung, J. W.; Liu, F.; Russell, T. P.; Jo, W. H. *Energy Environ. Sci.* **2012**, *5*, 6857–6861.
4. Selected examples: (a) Du, C.; Ye, S.; Chen, J.; Guo, Y.; Liu, Y.; Lu, K.; Liu, Y.; Qi, T.; Gao, X.; Shuai, Z.; Yu, G. *Chem.—Eur. J.* **2009**, *33*, 8275–8282; (b) Kumar, N. S.; Clement, J. A.; Mohanakrishnan, A. K. *Tetrahedron* **2009**, *65*, 822–830; (c) Hamwi, S.; Meyer, J.; Kroeger, M.; Winkler, T.; Witte, M.; Riedl, T.; Kahn, A.; Kowalsky, W. *Adv. Funct. Mater.* **2010**, *11*, 1762–1766.
5. Selected examples: (a) Kim, D. H.; Lee, B. L.; Moon, H.; Kang, H. M.; Jeong, E. J.; Park, J. I.; Han, K. M.; Lee, S.; Yoo, B. W.; Koo, B. W.; Kim, J. Y.; Lee, W. H.; Cho, K.; Becerril, H. A.; Bao, Z. *J. Am. Chem. Soc.* **2009**, *131*, 6124–6132; (b) DiBenedetto, S. A.; Facchetti, A.; Ratner, M. A.; Marks, T. J. *Adv. Mater.* **2009**, *21*, 1407–1433; (c) Lu, K.; Liu, Y. *Curr. Org. Chem.* **2010**, *14*, 2017–2033.
6. Selected examples: (a) Lu, P.; Lam, J. W. Y.; Liu, J. Z.; Jim, C. K. W.; Yuan, W. Z.; Chan, C. Y. K.; Xie, N.; Hu, Q.; Cheuk, K. K. L.; Tang, B. Z. *Macromolecules* **2011**, *44*, 5977–5986; (b) Li, S. Y.; Xu, Y. W.; Zeng, S. Q.; Xiao, L. M.; Duan, H. Q.; Lin, X. L.; Liu, J. M.; Su, C. Y. *Tetrahedron Lett.* **2012**, *53*, 2918–2921; (c) Algi, F. *Tetrahedron* **2013**, *69*, 3523–3529.
7. Selected examples: (a) Yildiz, H. B.; Toppare, L. *Biosens. Bioelectron.* **2006**, *21*, 2306–2310; (b) Pathak, R. K.; Hinge, V. K.; Mondal, M.; Rao, C. P. *J. Org. Chem.* **2011**, *76*, 10039–10049; (c) Wang, Y.; Liu, B. *Curr. Org. Chem.* **2011**, *15*, 446–464.
8. Selected examples: (a) Osken, I.; Bildirir, H.; Ozturk, T. *Thin Solid Films* **2011**, *519*, 7707–7711; (b) Padilla, J. *Sol. Energy Mater. Sol. Cells* **2012**, *99*, 56–61; (c) Khunchalee, J.; Tarsang, R.; Prachumrak, N.; Jungsuttiwong, S.; Keawin, T.; Sudyoadsuk, T.; Promarak, V. *Tetrahedron* **2012**, *68*, 8416–8423.
9. (a) *Electronic Materials: The Oligomer Approach*; Mullen, K., Wegner, G., Eds.; Wiley-VCH: Weinheim, Germany, 1998; (b) *Handbook of Thiophene-based Materials: Applications in Organic Electronics and Photonics*; Perepichka, I. F., Perepichka, D. F., Eds.; John Wiley & Sons: New York, NY, 2009.
10. Zade, S. S.; Zamoshchik, N.; Bendikov, M. *Acc. Chem. Res.* **2011**, *44*, 14–24.
11. Hou, Y. H.; Long, G. K.; Sui, D.; Cai, Y.; Wan, X. J.; Yu, A.; Chen, Y. S. *Chem. Commun.* **2011**, 10401–10403.
12. Chou, T. C.; Lin, K. C.; Kon-no, M.; Lee, C. C.; Shinmyozu, T. *Org. Lett.* **2011**, *13*, 4588–4591.
13. Wurthner, F.; Ahmed, S.; Thalacker, C.; Debaerdemaeker, T. *Chem.—Eur. J.* **2002**, *8*, 4742–4750.
14. Yamaguchi, E.; Shibahara, F.; Murai, T. *J. Org. Chem.* **2011**, *76*, 6146–6158.
15. Ellinger, S.; Graham, K. R.; Shi, P. J.; Farley, R. T.; Steckler, T. T.; Brookins, R. N.; Taranekar, P.; Mei, J. G.; Padilha, L. A.; Ensley, T. R.; Hu, H. H.; Webster, S.; Hagan, D. J.; Van Stryland, E. W.; Schanze, K. S.; Reynolds, J. R. *Chem. Mater.* **2011**, *23*, 3805–3817.
16. (a) Huang, W.; Masuda, G.; Maeda, S.; Tanaka, H.; Hino, T.; Ogawa, T. *Inorg. Chem.* **2008**, *47*, 468–480; (b) Wang, L.; You, W.; Huang, W.; Wang, C.; You, X. Z. *Inorg. Chem.* **2009**, *48*, 4295–4305; (c) Hu, B.; Fu, S. J.; Xu, F.; Tao, T.; Zhu, H. Y.; Cao, K. S.; Huang, W.; You, X. Z. *J. Org. Chem.* **2011**, *76*, 4444–4456; (d) Tao, T.; Peng, Y. X.; Huang, W.; You, X. Z. *J. Org. Chem.* **2013**, *78*, 2472–2481.
17. (a) Huang, W.; Masuda, G.; Maeda, S.; Tanaka, H.; Ogawa, T. *Chem.—Eur. J.* **2006**, *12*, 607–619; (b) Huang, W.; Tanaka, H.; Ogawa, T. *J. Phys. Chem. C* **2008**, *112*, 11513–11526; (c) Huang, W.; Tanaka, H.; Ogawa, T.; You, X. Z. *Adv. Mater.* **2010**, *22*, 2753–2758.
18. Coropceanu, V.; Cornil, J.; Da Silva Filho, D. A.; Olivier, Y.; Silbey, R.; Bredas, J. L. *Chem. Rev.* **2007**, *107*, 926–952 and references therein.
19. Sarma, M.; Chatterjee, T.; Ghanta, S.; Das, S. K. *J. Org. Chem.* **2012**, *77*, 432–444.
20. Ma, C. Q.; Pisula, W.; Weber, C.; Feng, X. L.; Mullen, K.; Bauerle, P. *Chem.—Eur. J.* **2011**, *17*, 1507–1518.
21. Turbiez, M.; Frere, P.; Roncali, J. *J. Org. Chem.* **2003**, *68*, 5357–5360.
22. Frisch, M. J.; Trucks, G. W.; Schlegel, H. B.; Scuseria, G. E.; Robb, M. A.; Cheeseman, J. R.; Scalmani, G.; Barone, V.; Mennucci, B.; Petersson, G. A.; Nakatsuji, H.; Caricato, M.; Li, X.; Hratchian, H. P.; Izmaylov, A. F.; Bloino, J.; Zheng, G.; Sonnenberg, J. L.; Hada, M.; Ehara, M.; Toyota, K.; Fukuda, R.; Hasegawa, J.; Ishida, M.; Nakajima, T.; Honda, Y.; Kitao, O.; Nakai, H.; Vreven, T.; Montgomery, J. A.; Peralta, J. E.; Ogliaro, F.; Bearpark, M.; Heyd, J. J.; Brothers, E.; Kudin, K. N.; Staroverov, V. N.; Kobayashi, R.; Normand, J.; Raghavachari, K.; Rendell, A.; Burant, J. C.; Iyengar, S. S.; Tomasi, J.; Cossi, M.; Rega, N.; Millam, N. J.; Klene, M.; Knox, J. E.; Cross, J. B.; Bakken, V.; Adamo, C.; Jaramillo, J.; Gomperts, R.; Stratmann, R. E.; Yazyev, O.; Austin, A. J.; Cammi, R.; Pomelli, C.; Ochterski, J. W.; Martin, R. L.; Morokuma, K.; Zakrzewski, V. G.; Voth, G. A.; Salvador, P.; Dannenberg, J. J.; Dapprich, S.; Daniels, A. D.; Farkas, O.; Foresman, J. B.; Ortiz, J. V.; Cioslowski, J.; Fox, D. J.; Gaussian, Inc.: Wallingford CT, 2009.
23. (a) Kuhn, H. *J. Chem. Phys.* **1949**, *17*, 1198–1212; (b) Taubmann, G. *J. Chem. Educ.* **1992**, *69*, 96–97; (c) de Melo, J. S.; Silva, L. M.; Arnaut, L. G.; Becker, R. S. *J. Chem. Phys.* **1999**, *111*, 5427–5433.
24. SMART and SAINT, Area Detector Control and Integration Software; Siemens Analytical X-ray Systems: Madison, WI, 2000.
25. Sheldrick, G. M. *SHELXTL (Version 6.10). Software Reference Manual*; Bruker AXS: Madison, WI, USA, 2000.